

# Cloud–Radiation Feedback and Atmosphere–Ocean Coupling in a Stochastic Multicloud Model

Yevgeniy Frenkel

*Department of Mathematics and Center for Atmosphere-Ocean Science, Courant Institute  
New York University  
251 Mercer Street  
New York, NY 10012 USA*

Andrew J. Majda

*Department of Mathematics and Center for Atmosphere-Ocean Science, Courant Institute ,  
and Center for Prototype Climate Modeling, NYU Abu Dhabi Institute  
New York University  
251 Mercer Street  
New York, NY 10012 USA*

Samuel N. Stechmann\*

*Department of Mathematics and Department of Atmospheric and Oceanic Sciences  
University of Wisconsin-Madison  
480 Lincoln Dr  
Madison, WI 53706*

---

## Abstract

Despite recent advances in supercomputing, current general circulation models (GCMs) have significant problems in representing the variability associated with organized tropical convection. Furthermore, due to high sensitivity of the simulations to the cloud radiation feedback, the tropical convection remains a major source of uncertainty in long-term weather and climate forecasts. In a series of recent studies, it has been shown, in the context of a paradigm two baroclinic mode system, that a stochastic multicloud convective parameterization based on three cloud types (congestus, deep and stratiform) can be used to improve the variability and the dynamical structure of tropical convection, including intermittent coherent structures such as synoptic and mesoscale convective systems.

---

\*Corresponding author

*Email address:* `stechmann@wisc.edu` (Samuel N. Stechmann )

Here, the stochastic multcloud model is modified with a parameterized cloud radiation feedback mechanism and atmosphere-ocean coupling. The radiative convective feedback mechanism is shown to increase the mean and variability of the Walker circulation. The corresponding intensification of the circulation is associated with propagating synoptic scale systems originating inside of the enhanced sea surface temperature area. In column simulations, the atmosphere ocean coupling introduces pronounced low frequency convective features on the time scale associated with the depth of the mixed ocean layer. However, in the presence of the gravity wave mixing of spatially extended simulations, these features are not as prominent. This highlights the deficiency of the column model approach at predicting the behavior of multiscale spatially extended systems. Overall, the study develops a systematic framework for incorporating parameterized radiative cloud feedback and ocean coupling which may be used to improve representation of intraseasonal and seasonal variability in GCMs.

*Keywords:* Stochastic convective parameterization, Multicloud models, tropical atmospheric dynamics, convectively coupled waves, cloud radiation feedback, atmosphere ocean coupling

---

## 1. Introduction

Atmospheric dynamics in the tropics are characterized by the predominance of organized convection on a wide range of scales, spanning mesoscale systems to synoptic and planetary-scale convectively coupled waves such as Kelvin waves and the Madden Julian oscillation (MJO)[1, 2, 3]. While the importance of the tropics to weather and climate forecast cannot be overestimated, present coarse resolution GCMs used for the prediction of weather and climate, have significant problems in representing variability associated with tropical convection[4, 5, 6, 7, 8].

It is believed that the deficiency is due to insufficient treatment of the cumulus convection [5, 9], which has to be parameterized in GCM. The inaccuracy of the vertical and horizontal cloud distributions furthers already great uncertainty

associated with the cloud radiation feedback (CRF) mechanisms [10, 11, 12, 13] and the large-scale atmospheric circulation [14, 15]. Given the sensitivity of tropical variability [10, 11, 12, 13] to CRF, the search for new strategies for the parameterization of tropical convection, associated radiative feedback and atmosphere ocean coupling (AOC) effects is one of the central problems in the atmospheric community.

Several methods have been developed to address the multiscale nature of the tropical convection. Cloud-resolving models (CRM) on fine computational grids have succeeded in representing some aspects of organized convection, including mesoscale organization and cloud distribution [16, 17, 18]. In addition, superparameterization (SP) methods [19, 20, 21, 22, 23] and sparse space-time SP [24, 25] use a cloud resolving model in each column of the large scale GCM to explicitly represent small scale processes, mesoscale processes and interactions between them. However, despite considerable success in duplicating observed radiative fluxes [26], these methods are not currently computationally viable for application to climate simulations. Neither do these complex models necessarily further the qualitative understanding of the processes involved. For example, CRF is usually computed through highly complex multiple-scattering and radiative transfer models [10, 27].

Another novel approach to the problem of missing tropical variability in GCMs has been the development of the multcloud parameterizations [28, 29, 30, 31, 32, 33, 34], which captures the interaction of the three cloud types (congestus, deep and stratiform) which characterize tropical convection. In particular, the stochastic multcloud model [33, 34, 35] (hereafter KBM10, FMK12, FMK13) aims to capture these phenomena with a Markov chain lattice model where each lattice site is either occupied by a cloud of a certain type or it is a clear-sky site. The convective elements interact with the large-scale environment and with each other through convective available potential energy (CAPE) and middle troposphere dryness. When local interactions between the individual lattice sites are ignored, the dynamical evolution of the cloud area fractions in the stochastic multcloud model takes the form of a computationally inexpensive coarse grained

stochastic process.[36, 37, 38]. Aside of enhanced representation of clouds, the  
45 framework is simple enough to allow semi-analytic solutions. In particular these  
authors were able to study stability and bifurcations of the solutions attribute to  
the diurnal surface fluxes [39]. Despite the apparent simplicity, the multcloud  
model is very successful in capturing most of the Wheeler-Kiladis-Takayabu  
50 spectrum of convectively coupled waves [40, 3] in terms of linear wave theory  
(KM06a,KM08b) and nonlinear organization of large-scale envelopes mimicking  
cross-scale interactions of the Madden-Julian oscillation (MJO) and convectively  
coupled waves (KM07; KM08a; [41]), in the idealized context of a simple two-  
baroclinic modes model employed here. Both the deterministic and stochastic  
multcloud models dramatically improve the representation of the coherent and  
55 intermittent nature of organized convection. This has been shown in an idealized  
two baroclinic mode framework coupled to a coarse resolution GCM for both  
the MJO and monsoon intraseasonal oscillations. [42, 43, 44, 45, 43]. .

Here, a version of the stochastic multcloud parameterization (FMK13) is  
augmented with cloud radiation feedback and ocean coupling mechanism. As in  
60 FMK13, the parameterization is coupled to a simplified model of the primitive  
equations; the vertical resolution is reduced to the first two baroclinic modes.  
The impact of radiative convective feedback of each of the three cloud type  
is parameterized through a product of the cloud fraction and two parameters,  
which represent idealized projection of the effect onto the two baroclinic modes  
65 of the system. The radiative feedback is shown to increase the strength and  
variability of Walker circulation. The atmosphere-ocean coupling increases the  
variability of convection by introducing low frequency envelopes of synoptic  
and mesoscale convective systems. Single column simulations are used here  
to isolate and elucidate the effects of these modifications. Atmosphere-ocean  
70 coupling and cloud radiation feedback have a subtle but significant effect in  
spatially extended simulations. Spectral analysis highlights the effects of the  
modifications introduced here and their interactions with intrinsic variability  
of the system. The study is intermediate between overly simple one baroclinic  
mode models [15, 46] and more complex GCM and CRM simulations [27, 5].

75 The remainder of the paper is organized as follows. A self-contained review of the stochastic multcloud parameterization is presented in Section 2. The section also introduces cloud radiation feedback and atmosphere ocean coupling mechanisms. In Section 3, single column simulation are used to illustrate the effects of the two modifications listed above. In Section 4, the modified parameterization is used to study flows above the equator in a series of idealized Walker  
80 cell simulations. Some discussion and concluding remarks are given in Section 5.

## 2. Multicloud model, cloud radiation feedback and atmosphere-ocean coupling

85 We start with a brief review of the dynamical core equations used for the stochastic multcloud parameterization in Section 2.1. A more thorough and detailed discussion of the model equations is found in (KM06). Nevertheless, a comprehensive list of the model constants and parameters is given in Table 1 for the sake of completeness. Section 2.2 reviews the stochastic multcloud parameterization, while Sections 2.3 and 2.4 introduce cloud radiative feedback  
90 and ocean coupling, respectively.

### 2.1. Dynamical core

The stochastic multcloud parameterization assumes three heating profiles associated with the main cloud types that characterize organized tropical convective systems [47]: cumulus congestus clouds that heat the lower troposphere  
95 and cool the upper troposphere, through radiation and detrainment, deep convective towers that heat the whole tropospheric depth, and the associated lagging-stratiform anvils heat the upper troposphere and cool the lower troposphere, due to evaporation of stratiform rain. Accordingly, the dynamical core used in this paper consists of two coupled and forced shallow water systems.  
100 Without the meridional dependency, the equations are given by

$$\partial_t u_j - \partial_x \theta_j = C_d u_0 u_j - \frac{1}{\tau_R} u_j, \quad j = 1, 2 \quad (1)$$

$$\partial_t \theta_1 - \partial_x u_1 = H_d + \xi_s H_s + \xi_c H_c + S_1, \quad (2)$$

$$\partial_t \theta_2 - \frac{1}{4} \partial_x u_2 = H_c - H_s + S_2. \quad (3)$$

Here  $H_d, H_s$  and  $H_c$  are the heating rates for deep, stratiform and cumulus congestus clouds obtained by either the deterministic or the stochastic parameterization. These heating rates are combined to form the bulk precipitation  $P = H_d + \xi_s H_s + \xi_c H_c$ . The coefficients  $\xi_c$  and  $\xi_s$  denote contribution of congestus and stratiform rain to the bulk precipitation. The parameters  $C_d$  and  $u_0$  are respectively the momentum drag coefficient and the strength of turbulent fluctuations in the boundary layer. The last terms of the first and second baroclinic heating mode equations,  $S_j, j = 1, 2$ , represent cloud radiation cooling effects and will be discussed in Section 2.3.

The multcloud models additionally carry an equation for the vertically integrated tropospheric moisture content,  $q$ , and an equation for the boundary layer equivalent potential temperature,  $\theta_{eb}$ .

$$\partial_t q + \partial_x [(u_1 + \tilde{\alpha} u_2)q + (u_1 + \tilde{\lambda} u_2)\tilde{Q}] = -\frac{2\sqrt{2}}{\pi} P + D/H_T \quad (4)$$

$$\partial_t \theta_{eb} = \frac{1}{h_b} (E - D). \quad (5)$$

The sea surface saturation equivalent potential temperature,  $\theta_{eb}^*(T_s)$ , is function of bulk ocean layer temperature discussed in Section 2.4. For simulations without AOC,  $\theta_{eb}^*(T_s)$  is set to constant, so that  $\bar{\theta}_{eb}^* - \bar{\theta}_{eb} = 10K$ . Here and throughout the paper,  $\bar{X}$  denotes the RCE value of the variable  $X$ . In the  $(x, t)$  simulations where SST is not homogenous, the sea surface evaporation  $E$  takes the form

$$\frac{E}{h_b} = \tau_e^{-1} (\theta_{eb}^*(T_s) + \theta_{eb\Delta}^*(x) - \theta_{eb}). \quad (6)$$

the sea surface saturation equivalent potential temperature takes the form

$$\theta_{eb\Delta}^*(x) = 5 \cos\left(\frac{4\pi x}{40000}\right) + 10K, \quad (7)$$

within an interval of 20,000 km of the 40,000 km domain and  $\theta_{eb}^* = 5$  K everywhere else as in Khouider and Majda (2007) and KM08a. This setup mimics the Indian Ocean–Western Pacific warm pool.

Parameter	Value	Description
$h_b/H_m/H_T$	500 m / 5 km/ 16 km	depth of ABL/ mid-troposphere/ free troposphere
$\xi_s/\xi_c$	0.4/0	Stratiform/Congestus contribution to first baroclinic mode
$\bar{Q}$	0.9	Background moisture stratification
$\tilde{\lambda}/\tilde{\alpha}$	0.8/0.1	Coefficient of $u_2$ in linear / nonlinear moisture convergence
$m_0$	Determined at RCE	Large-scale background downdraft velocity scale
$\mu$	0.25	Contribution of convective downdrafts to $D$
$\alpha_s/\alpha_c$	0.25/ 0.1	Stratiform/Congestus adjustment coefficient
$\tau_R/\tau_D$	75 days / 50 days	Rayleigh drag / Newtonian cooling time scale
$\tau_s/\tau_c$	3 hours / 2 hour	Stratiform /Congestus adjustment time scale
$\tau_{conv}$	2 hours	Convective time scale
$\tau_e$	Determined by RCE	Surface evaporation time scale
$\bar{Q}$	Determined at RCE	Bulk convective heating at RCE
$\bar{\theta}_{eb} - \bar{\theta}_{em}$	11 K	Mean (RCE) Dryness of the atmosphere
$a_1/a_2$	0.45 / 0.55	Relative contribution of $\theta_{eb}$ / $q$ to deep convection
$a_0/a'_0$	2 / 1.5	Dry convective buoyancy frequency in deep/congestus eqns.
$\gamma_2/\gamma'_2$	0.1 / 2	Relative contribution of $\theta_2$ to deep /congestus heating
$\alpha_2$	0.1	Relative contribution of $\theta_2$ to $\theta_{em}$
$C_d$	0.001	Surface drag coefficient
$u_0$	2 m/s	Strength of turbulent fluctuations
$CAPE_0$	400 J/Kg	Reference values of CAPE
$T_0$	12 K	Reference values of dryness
$\bar{\alpha}$	$\approx 15$ K	Unit scale of temperature
$R_{univ}$	$\approx 8.31436$ J/mole K	Gas constant (universal)
$R_d$	$\approx 287.04$ J/kg K	Gas constant (dry air)
$R_v$	$\approx 1461.50$ J/kg K	Gas constant (water vapor)
$T_{ref}$	$\approx 301$ K	Constant reference temperature
$L_v$	$\approx 2.435 \cdot 10^6$ J/kg	Latent heat of vaporization
$c_p$	$\approx 1005$ J/K kg	Heat capacity of dry air

Table 1: Constants and parameters for multcloud parameterizations.

Description	Expression
Midlevel $\theta_{em}$	$\theta_{em} = q + \frac{2\sqrt{2}}{\pi}(\theta_1 + \alpha_2\theta_2)$
Precipitation	$P = H_d + \xi_s H_s + \xi_c H_c$
Downdrafts	$D = m_0(1 + \mu(H_s - H_c)/Q_{R01})^+(\theta_{eb} - \theta_{em})$
Radiation	$Rad_1 = Q_{R01} - \frac{\theta_1}{\tau_D}$ , and $Rad_2 = Q_{R02} - \frac{\theta_2}{\tau_D}$
CAPE	$CAPE = \overline{CAPE} + R(\theta_{eb} - \gamma(\theta_1 + \gamma_2\theta_2))$
Lower level CAPE	$CAPE_l = \overline{CAPE} + R(\theta_{eb} - \gamma(\theta_1 + \gamma'_2\theta_2))$
Deep heating	$H_d = \left[ \sigma_d \bar{Q} + \frac{\sigma_d}{\bar{\sigma}_d \tau_c^0} (a_1 \theta_{eb} + a_2 q - a_0 (\theta_1 + \gamma_2 \theta_2)) \right]^+$
Congestus heating	$H_c = \sigma_c \frac{\alpha_c \bar{\alpha}}{H_m} \sqrt{CAPE_l^+}$

Table 2: Summary of important diagnostic quantities in multicloud model. For more details, the reader is referred to FMK13.

## 2.2. Stochastic multicloud parameterization

The stochastic multicloud parameterization is designed to capture the dynamical interactions between the three cloud types that characterize organized tropical convection and the environment. In the stochastic multicloud model these interactions are represented through a coarse grained lattice model (KBM10).  
130 To mimic the behavior within a typical GCM grid box, a rectangular  $n \times n$  lattice is considered. Each element of the lattice is occupied by a congestus, deep or a stratiform cloud or is a clear sky site. It is represented by an order parameter that takes accordingly the values 0,1,2 or 3. A continuous time stochastic process is then defined by allowing the transitions, for individual cloud sites, from  
135 one state to another according to intuitive probability transition rates, which depend on the large scale-resolved variables. These large scale variables are the convective available potential energy integrated over the whole troposphere (CAPE), low level CAPE (see Table 2) and the dryness of the mid troposphere,  
140 which is a function of the difference between the atmospheric boundary layer

Table 3: Transition rates and time scales in the stochastic multicloud model simulations. Here  $\Gamma(x) = 1 - \exp(-x)$  for  $x > 0$  and zero otherwise,  $C_l = CAPE_l/CAPE_0$ ,  $C = CAPE/CAPE_0$  and  $D = (\theta_{em} - \theta_{eb})/T_0$ . For more details, the reader is referred to FMK13.

Description	Transition Rate	Time scale (h)
Formation of congestus	$R_{01} = \frac{1}{\tau_{01}} \Gamma(C_l) \Gamma(D)$	$\tau_{01}=1$
Decay of congestus	$R_{10} = \frac{1}{\tau_{10}} \Gamma(D)$	$\tau_{10}=1$
Conversion of congestus to deep	$R_{12} = \frac{1}{\tau_{12}} \Gamma(C)(1 - \Gamma(D))$	$\tau_{12}=1$
Formation of deep	$R_{02} = \frac{1}{\tau_{02}} \Gamma(C)(1 - \Gamma(D))$	$\tau_{02}=3$
Conversion of deep to stratiform	$R_{23} = \frac{1}{\tau_{23}}$	$\tau_{23}=3$
Decay of deep	$R_{20} = \frac{1}{\tau_{20}} (1 - \Gamma(C))$	$\tau_{20}=3$
Decay of stratiform	$R_{30} = \frac{1}{\tau_{30}}$	$\tau_{30}=5$

(ABL) temperature  $\theta_{eb}$  and the middle tropospheric potential temperature  $\theta_{em}$ . The inclusion of the dryness of the middle troposphere accounts for mixing of the convective parcels with dry environmental air is conceptually similar to the switch  $\Lambda$  in the deterministic multcloud model (KM06a, KM06b, KM07, KM08a, KM08b).

The probability rates are constrained by a set of intuitive rules which are based on observations of cloud dynamics in the tropics (e.g. [47, 48], KM06a, and references therein). Following KBM10, a clear site turns into a congestus site with high probability if low level CAPE is positive and the middle troposphere is dry. A congestus or clear sky site turns into a deep convective site with high probability if CAPE is positive and the middle troposphere is moist. A deep convective site turns into a stratiform site with high probability. Finally, all three cloud types decay naturally to clear sky at some fixed rate. All other transitions are assumed to have negligible probability. These rules are formalized in Table 3. Notice that the assumption that the transition rates depend on the large scale variables accounts for the feedback of the large scales on the stochastic model, while ignoring the interactions between the lattice sites all together implies that the stochastic processes associated with the different sites are identical (independent and identically distributed). The latter simplification makes it easy to derive the stochastic dynamics for the GCM grid box cloud coverage alone, which can be evolved without the detailed knowledge of the micro-state configuration, by using a coarse-graining technique [36, 49] that yields here a system of three dimensional birth-death stochastic process for the congestus, deep and stratiform cloud fractions  $\sigma_c, \sigma_d$  and  $\sigma_s$  respectively. The cloud fractions impact the large scale dynamics through algebraic congestus and deep heating closures, listed in Table 2, and dynamical closure for stratiform heating below,

$$\partial_t H_s = \frac{1}{\tau_s} (\alpha_s \sigma_s H_d / \bar{\sigma}_d - H_s). \quad (8)$$

More detailed description of the stochastic multcloud model can be found in FMK13.

170 *2.3. Cloud Radiation Feedback*

Clouds plays a key role in the understanding weather and climate. The stochastic multcloud model outlined in the previous section does a remarkable job of capturing the distributions of the three cloud types (congestus, deep and stratiform) that characterize tropical convection in a paradigm two baroclinic mode system. Here we augment the stochastic multcloud model by addition of radiative convective feedback. The impact of radiative convective feedback of each of the three cloud type is parameterized through a product of the cloud fraction and two parameters, which represent idealized projection of the effect onto the two baroclinic modes of the system. The physical motivation for the CRF parameterization is outlined below.

Generally, low and thick clouds, such as congestus, primarily reflect solar radiation and cool the surface of the Earth. The radiative fluxes within the deep convective clouds primarily cancel but result in slight warming. High, thin clouds, such as stratiform clouds, transmit some of the incoming solar radiation; at the same time, they trap some of the outgoing infrared radiation emitted by the Earth and radiate it back downward, thereby warming the surface of the Earth and atmosphere below. In this simple framework we will assume stratiform clouds (due to their relative thinness) transmit half of the short wave radiation of the congestus or deep clouds. The degree of cooling or heating of cloud depends on several factors, including the cloud's altitude, its size, and the make-up of the particles that form the cloud, such as ice and aerosols. Here we are primarily concerned with effect of three idealized paradigm cloud types and their impact upon the two baroclinic modes of the system. We are guided by our intuitive understanding of clouds and observational evidence below.

As noted by [50], observations based on Earth Radiation Budget Experiment (ERBE) satellite data indicate that there is a near cancellation of fluxes between tropical long wave and shortwave cloud forcing in regions of deep convective activity. We define cloud radiative forcing as the difference between the radiative heatings for cloud and clear skies. Positive cloud forcing implies the presence of the cloud warms the atmosphere relative to a clear sky heating profile. In

oder to infer the effects of cloud radiative forcing, we consider the observations studies [51, 52]

As shown in observations of [51] and CRM studies [14], within the deep cloud, the longwave and shortwave heating are both essentially zero. The long-  
 205 wave cooling at cloud top apparently overwhelms the shortwave warming there, and the result is slight cooling in the first baroclinic mode and more cooling in the upper troposphere than the lower troposphere. For stratiform and deep convective clouds, longwave cloud top cooling is roughly balanced by shortwave cloud top warming during daytime. As result deep convective clouds warm the  
 210 lower troposphere relative to the upper troposphere due to longwave cloud base warming in the lower troposphere [51, 52]. This results in the positive projection onto both first and second baroclinic modes to create a heating profile biased towards lower troposphere. By the same reasoning [51, 52, 14], stratiform clouds, which follow the deep convection, warm the upper troposphere  
 215 relative to the lower troposphere due to longwave cloud base warming in the upper troposphere. This corresponds to the choice of heating profile slightly biased towards upper level heating through negative second baroclinic mode contribution. The evidence for effects of congestus cloud forcing is less clear [52]. The congestus clouds do not extend in the upper troposphere, and therefore  
 220 the forcing here is zero. The observational evidence [53] points to wards cooling of the lower troposphere relative to the upper troposphere by congestus clouds due to longwave cloud top cooling. This corresponds to cooling in of both first and second baroclinic modes by congestus radiative feedback.

The cloud radiative forcing inferred from the observations above is projected  
 225 on two the baroclinic modes of variability in the model. Formally, we propose the following parameterization for radiative flux terms  $S_i, i = 1, 2$  in equations 1 :

$$S_i = -\theta_i/\tau_D + \sigma_{cs}R_i^{clear} + (\sigma_c R_i^c + \sigma_d R_i^d + \sigma_s R_i^s)\alpha, i = 1, 2 \quad (9)$$

Here,  $\sigma_{cs} = 1 - \sigma_c - \sigma_d - \sigma_s$ , is clear sky fraction. We also introduce tuning parameter,  $\alpha$ . Setting  $\sigma_{cs} = 1$  and  $\alpha = 0$  reduces radiative flux to a simpler

230 formulation,  $S_i = \theta_i/\tau_D + R_i^{clear}$ , which is use all previous iterations of the  
 multcloud model. As was the case with FMK13 , the value of  $R_1^{clear} = -1$   
 K/day is used for first baroclinic mode heating. The value of  $R_2^{clear}$  is set  
 by RCE and is on order of half of Kelvin per day. We choose to combine  
 the short wave and longwave cloud radiative effect. In particular, we suppress  
 235 the role of the short-wave fluxes as their calculation would necessitate complex  
 compositions involving incoming and outgoing radiation and solar zenith angle.  
 Plots of the cloud forcing and cloud radiation heating rate profiles for particular  
 choice of parameters in Table 4 are shown in Figure 1. Left panel of the figure  
 shows idealized convective heating of the three cloud types. Since there is no  
 240 congestus precipitation in this parameter regime ( $\xi_c = 0$ ), congestus heating  
 projects purely on second baroclinic mode, warming lower troposphere (and  
 cooling upper troposphere). Deep convection projects only on the first baroclinic  
 mode, warming the mid-troposphere. Stratiform rain projects onto the first  
 baroclinic, through,  $\xi_s = 0.5$ , in addition to warming the upper troposphere  
 245 and cooling (through evaporation) of lower troposphere. This results in the  
 profile skewed towards the upper troposphere heating. The right panel shows  
 schematics of cloud radiative forcing profile computed from each cloud type and  
 clear sky. The schematic is computed by imposing values in Table 4 on the  
 two baroclinic modes and (for ease of comparison) assuming that each cloud  
 250 completely covers the sky. The cloud forcing profiles are similar to the ones  
 used by [53] (see Figure 11 of that study) to process Tropical Rainfall Measuring  
 Mission (TRIMM). The formulation above is also based on the GATE (GARP  
 Atlantic Tropical Experiment) data studies [51, 52]. The clear sky cooling  
 rate is comparable to the values used in previous multcloud model studies.  
 255 Lastly, this type of direct CRF parameterization, where CRF is assumed to be  
 proportional to cloud fraction or heating (often through precipitation efficiency  
 parameter), is commonly a part of the radiation scheme in both simple one  
 baroclinic mode model [46] and CRM studies [13, 27].

Table 4: Parameters and constants used for the cloud radiative feedback and ocean coupling. Note that  $R_2^{clear} \approx 0.3$  K/Day is determined by RCE and is comparable to the value used in the previous multcloud model studies.

Parameter	CRF rate coefficient associated with	value
$R_1^c$	Congestus clouds for 1st baroclinic mode	-3 K/day
$R_1^d$	Deep clouds for 1st baroclinic mode	6 K/day
$R_1^s$	Stratiform clouds for 1st baroclinic mode	6 K/day
$R_1^{clear}$	Clear sky for 1st baroclinic mode	-1 K/day
$R_2^c$	Congestus clouds for 2nd baroclinic mode	-1.5 K/day
$R_2^d$	Deep clouds for 2nd baroclinic mode	3 K/day
$R_2^s$	Stratiform clouds for 2nd baroclinic mode	-3 K/day
$R_2^{clear}$	Clear sky for 2nd baroclinic mode	-0.2 K/day

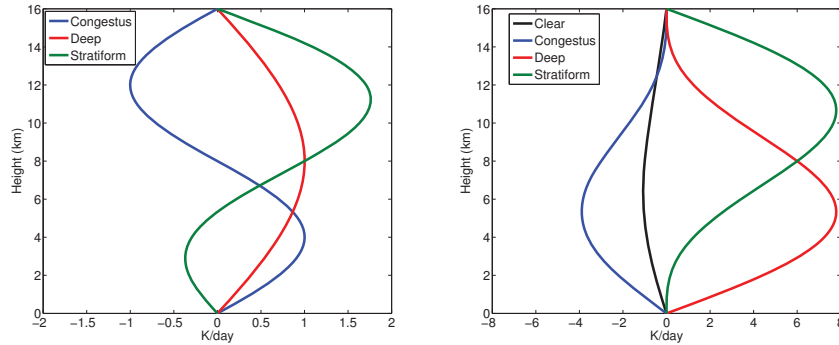


Figure 1: Left: Idealized convective heating of the three cloud types. Since there is no congestus precipitation in this parameter regime ( $\xi_c = 0$ ), congestus heating projects purely on second baroclinic mode. Deep convection projects only on the first baroclinic mode. Stratiform rain projects onto the first baroclinic (through  $\xi_s = 0.5$ ) in addition to warming the upper troposphere, thus resulting in profile skewed towards the upper troposphere heating. Right: schematics of cloud radiative forcing profile computed from each cloud type and clear sky. The schematic is computed by imposing values in Table 4 on the two baroclinic modes and (for ease of comparison) assuming that each cloud completely covers the sky. The clear sky cooling rate is of profile typically used in the multcloud models.

#### 2.4. Slab mixed-layer ocean

260 We use a simple model for an interactive bulk mixed-layer ocean. The character of our mixed-layer ocean will be subsumed into a single variable,  $T_s$ , the sea surface mixed layer temperature. The evolution of  $T_s$  will be given by

$$c_0 \frac{dT_s}{dt} = S - \frac{c_0}{\tau_{eo}} (\theta_{eb}^*(T_s) - \theta_{eb}) \quad (10)$$

where  $c_o$  is the heat capacity for the mixed layer ocean. The radiation flux,  $S = S^{rad} + S^{out}$ , includes radiative effects,  $S = S^{rad}$  and an imposed ocean  
 265 heat transport,  $S^{out}$ . The ocean layer evaporation constant,  $\tau_{eo}$  is constrained by RCE so that  $\overline{T_s} = 0$ . The sensible heat flux will be ignored, since its contribution to the energy budget is small compared to the shortwave radiation and latent heat fluxes [14, 46, 54, 39].

In their model for Walker circulation, [46] used a similar mixed-layer ocean  
 270 model. The authors used zonally varying term for the combined effect of ocean  
 heat transport and clear sky shortwave forcing. Also, a similar model with  
 zonally varying ocean heat transport has been used in [14]. Here, we omit  
 explicit representation of the ocean heat transport and instead use equation  
 7 to account for zonal SST variation implicitly, through  $E$ . This facilitates a  
 275 direct comparison to previous multcloud studies.

As shown in [14, 46], the long-wave cooling of the surface is nearly cancelled  
 by back radiation from the atmosphere. Due to the smallness of longwave cloud  
 forcing we will not consider long-wave radiation for cloud forcing at the surface,  
 but will include long-wave effects in the constant clear sky flux. For the radiative  
 280 flux  $S^{rad}$  at the surface, we will have a clear sky component  $S^{clear}$  and a cloud  
 forcing component  $S^{cf}$  :

$$S^{rad} = S^{clear} + S^{cf} \quad (11)$$

For clear sky, the net shortwave flux averaged over one day is roughly  
 $S^{clear} = 300 \text{ W/m}^2$ , as shown in [46]; and the net long-wave flux is roughly  $S_{lw}^{clear}$   
 $= -50 \text{ W/m}^2$ , as shown in [14]. Therefore, we will choose the daily-averaged clear  
 285 sky flux to be

$$S^{clear} = S_{lw}^{clear} + S_{sw}^{clear} \quad (12)$$

For the radiative cloud forcing, we use

$$S^{cf} = -S_{sw}^{clear}(\sigma_c + \sigma_d + 0.5\sigma_s) \quad (13)$$

In the equation above, we make an assumption that stratiform clouds, due to  
 their relative thinness, block half of the radiation of the thicker congestus and  
 deep clouds. However, a large area fraction of stratiform clouds makes them  
 290 extremely important for radiative feedback effects.

We can further rewrite equation 10 in an explicit form.

$$\frac{dT_s}{dt} = \frac{S^{clear}(1 - A^c) - S^{sw} A^c}{c_0} - \frac{1}{\tau_{eo}}(\theta_{eb}^*(T_s) - \theta_{eb}) \quad (14)$$

Here we use the sum of cloud area fractions to determine fraction cloud coverage of the sky  $A^c = (\sigma_c + \sigma_d + 0.5\sigma_s)\alpha_o$ , along with a tuning parameter  $\alpha_o$ . This running parameter is similar to tuning parameter  $\alpha$  used for radiative feedback coupling. The corresponding radiative factor for convective clouds is given by  $S^{sw} \approx 200 \text{ W/m}^2$ , as estimated above. The mixed layer heat capacity  $c_0$ , give by

$$c_0 = c_{R,0}\rho_0 h_{ml} \quad (15)$$

This calculation is based on (heat capacity)  $c_{R,0} = 4000 \text{ J/kg K}$  and density  $\rho$ . When depth of mixed layer,  $h_{ml}$ , is set to 20 meters,  $c_0 \approx 8 \times 10^7 \text{ JK}^{-1} \text{ m}^{-2}$ . This mixed layer depth corresponds to approximately 40 day time scale for mixed ocean layer. In select simulations presented here, we will vary mix layer depth, by setting  $h_{ml} = 10, 20$  and 40 meters, which results in AOC time scale of 20, 40 and 80 days, respectively, for mixed layer. The ocean layer  $T_s$  is coupled to the atmospheric boundary layer ( $\theta_{eb}$ ) through atmospheric boundary layer saturation equivalent potential temperature. A simple closure,  $\theta_{eb}^*(T_s) = 5T_s$ , is derived from Clausius–Clapeyron relation in Appendix A. In simulations without ocean, saturation equivalent potential temperature,  $\theta_{eb}^*$ , is independent of  $T_s$ .

### 3. Single column simulations

In this section, the effects of the new mechanisms of cloud-radiation feedback and atmosphere-ocean coupling, are studied in the context of single column simulations and compared to the FMK13 results. The single column equations are obtained by disregarding spatial dependence components and the zonal wind. As in KBM10, we employ a third order Adams-Bashforth method to integrate the dynamical core ODEs. The coarse grained birth-death process is evolved in time by means of Gillespie’s exact algorithm [55, 56]. All simulations in this section are run for 2000 days, while a 10 or 100 days interval of the solution is shown.

To facilitate the comparison, we first review the basic results of FMK13.  
320 Figure 2 show the stochastic simulation of FMK13. The most notable feature is  
the time synchronization of the oscillations of the stochastic and deterministic  
variables which leads to time series with frequent precipitation peaks of 10  
K/Day and more intermittent large precipitation events on the order of 20  
K/Day. Each convective even is initialized by a build up of low level CAPE.  
325 The resulting congestus clouds moisten the atmosphere. This moist atmosphere,  
combined with the build up of CAPE, produces deep convective events which are  
in turn followed by stratiform clouds. The relationship between small and large  
precipitation events is reminiscent of a progressive deepening of convection on  
multiple scales (Mapes et al. 2006). By design, the congestus clouds are followed  
330 by deep convective and trailing stratiform clouds. The transitions rates are  
associated with moisture and dryness. In particular, we see a high correlation  
between positive,  $\theta_{eb}$  and moisture anomalies and deep convective activities. In  
this simulation, the ocean mixed layer temperature equation is slaved to the  
atmospheric variables and does not feedback into the model dynamics.

335 Figures 3 shows the time series of simulations with cloud radiation feedback  
and atmosphere ocean layer and with radiative convective feedback. We choose  
small value of CRF strength ( $\alpha = 0.1$ ) and 40 meter deep ocean layer. The  
top panel shows the contribution of the radiative feedback to the heating. The  
effects of radiative convective feedback are subtle. The feedback accounts for  
340 roughly one tenths of the heating in the column, which most significant contri-  
bution coming from large deep convective events and trailing stratiform anvils.  
On the other hand, the atmosphere ocean coupling produces pronounced enve-  
lope of convective activity with roughly 30 day period of oscillation (as will be  
shown in the following figures), associated with the ocean temperature fluctua-  
345 tions (bottom panel). The clear sky conditions lead to increase in mixed ocean  
layer temperature, which leads to increase in ABL temperature anomalies, and  
creation of deep convection and stratiform anvils, which cools mixed ocean layer,  
in turn, leading to smaller convective fraction and clear sky, closing the loop.  
Overall, the dynamics of the model becomes more irregular with introduction

350 of ocean coupling and CRF. In fact the model has suppressed and enhanced  
convection periods associated with time scale related to the ocean depth. The  
direct link between the ocean layer depth and the intraseasonal and seasonal  
oscillations will be discussed in detail. These oscillations resemble suppressed  
and active phases of MJO but on different time scales. We note that, just like  
355 in MJO, the suppressed phase of oscillation has intermittent deep convection  
and small average cloud fraction, while the active phase of oscillation consists  
of highly organized coherent convective episodes.

In Figure 4 we study the response of the model to variation in the strength  
of the CRF in presence of the 20 meter deep ocean layer coupling. For reference,  
360 panel A shows results from FMK13 (see Figure 3 in FMK13). The mixed ocean  
layer is added in simulations of panel B, we note that ocean coupling introduces  
weak low frequency envelope to the time series. It can be seen that the period of  
oscillation is on order of 30 days. The addition of weak CRF coupling ( $\alpha = 0.1$ ),  
in panel C, enhances this effect but shortens the frequency of the oscillation. It  
365 also makes oscillations in the ocean mixed layer more chaotic. The strong CRF  
coupling ( $\alpha = 0.4$ ), of panel D, destroys the low frequency envelope. The values  
of  $\alpha$  higher than approximately 0.4 produce unphysical large climatology. This  
is similar to the findings of [46], where the critical values of convective feedback  
tuning parameter were also documented.

370 In Figure 3, we experiment with the depth of the ocean mixed layer, while  
keeping the cloud radiation feedback constant (at weak value of  $\alpha = 0.1$ ). It  
appears that the mixed ocean layer envelope modulation is prominent for all  
ocean depths considered. We also observe that as depth of the ocean layer  
is proportional to the period of oscillation of mixed ocean layer temperature  
375 anomalies. To quantify the changes in the behavior we study the Fourier spec-  
trum of the precipitation in Figure 5. Firstly, we observe that ocean coupling  
introduces low frequency oscillation. It could further be established that the  
time scale of this oscillation is proportional to the depth of the layer. Secondly,  
we draw the conclusion that strong convective radiative feedback interferes with  
380 the low frequency introduced by the ocean mixed layer. The stronger values of

radiative feedback lead to shift of the power in the spectrum from low frequency oscillations associated with ocean layer to higher frequency intrinsic variability. While the results are omitted for conciseness, in absence of ocean coupling, radiative feedback slightly shifts the power spectrum towards the modes with  
385 frequency slightly lower than the intrinsic variability of the system but shorter than frequencies associated with bulk ocean layer. The Fourier spectrum analysis confirms observations made from Figure 4.

It is believed that both CRF and AOC play an important role in low frequency tropical variability, such as MJO and ENSO [13]. However, it is hard  
390 to infer the exact effects of CRF and AOC on these multiscale phenomena from column simulations. In order to investigate the behavior of the model further we proceed to the spatially extended simulations.

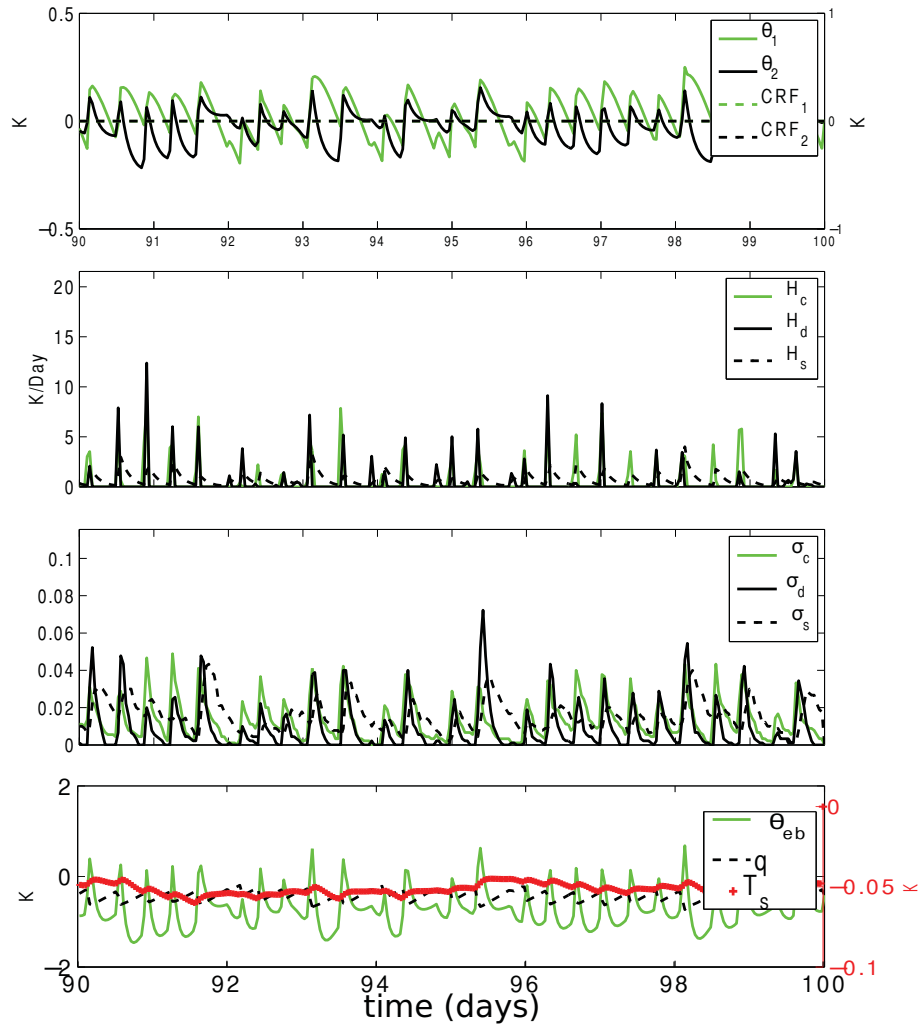


Figure 2: Time series of dynamic variables for FMK13 . In this simulation, the ocean mixed layer temperature equation is a passive slave to the system and does not feedback into the model dynamics.

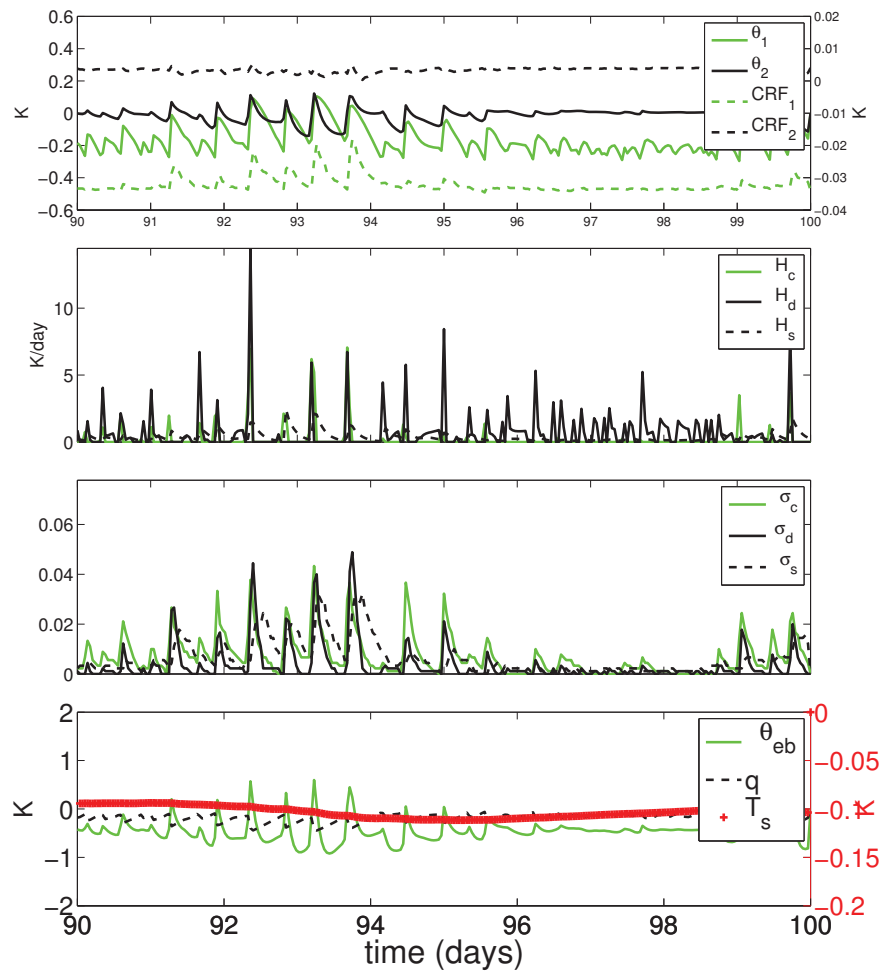


Figure 3: FMK13  $\alpha = 0.1$  with 40 meter deep ocean layer . The effects of radiative convective feedback accounts for roughly one tenths of the heating in the column. Overall, the dynamics of the model is greatly improved by the introduction of the suppressed and enhanced convection periods associated with low frequency sea surface temperature oscillations.

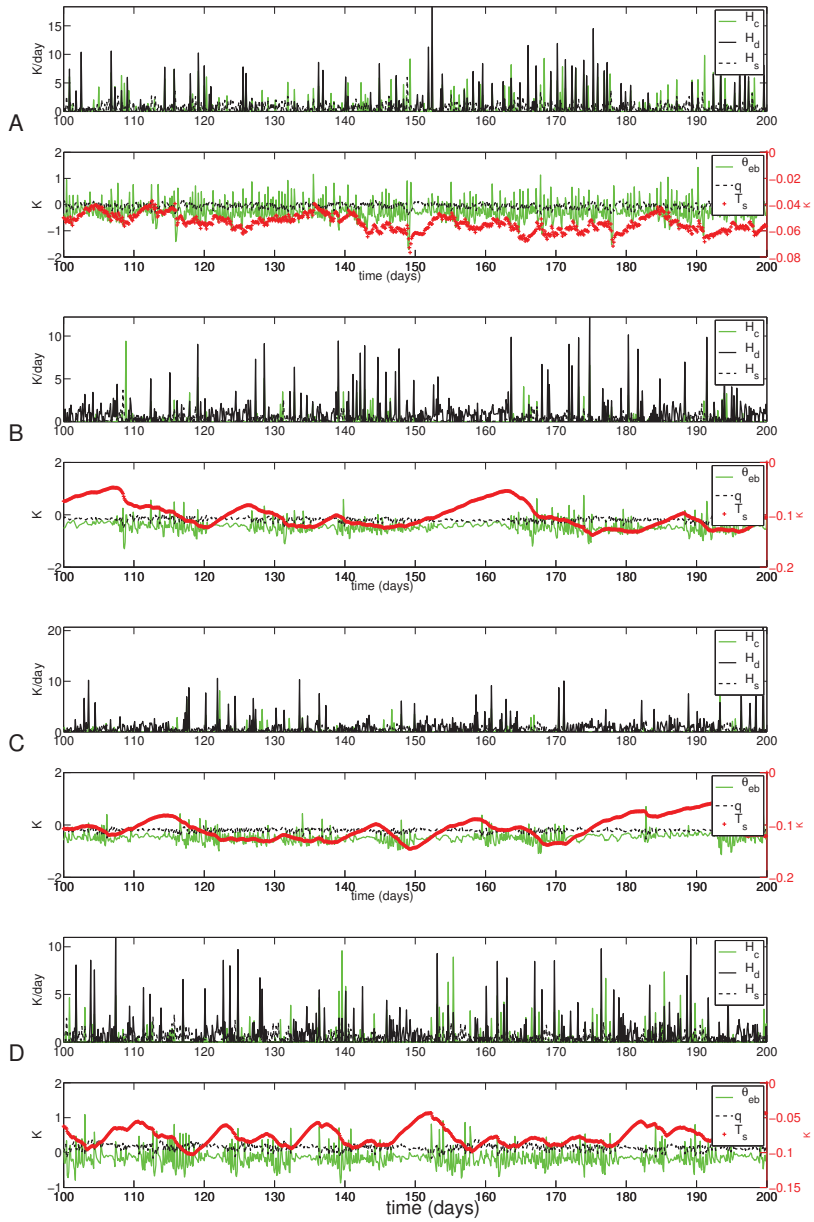


Figure 4: Precipitation and mixed ocean layer temperature for simulations (top to bottom) associated with: A) FMK13, simulations with atmosphere ocean coupling (20 meter) and B) without radiative feedback  $\alpha = 0$ , C) with weak feedback  $\alpha = 0.1$  and D) with strong radiative feedback  $\alpha = 0.4$ .

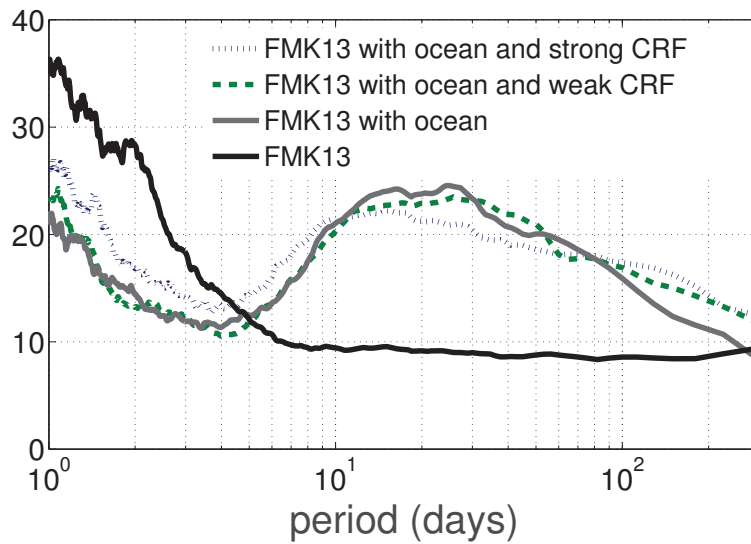


Figure 5: Power spectrum of precipitation time-series for column simulations with FMK13 (solid black), FMK13 with atmosphere-ocean coupling (20 meter) and without radiative feedback  $\alpha = 0$  (solid grey), FMK13 with atmosphere-ocean coupling (20 meter) and with weak radiative feedback  $\alpha = 0.1$  (green dash) and FMK13 with atmosphere-ocean coupling (20 meter) and with weak radiative feedback  $\alpha = 0.4$  (fine blue dash). This corresponds to four cases shown in Figure 4.

RCF	Ocean	SST	(U ,W )	std( $u_1$ )
$\alpha$			(m/s,cm/s,)	m/s
0	-	5K	(9.3 ,0.86 )	0.18
0.1	-	5K	(9.7 ,0.97 )	0.19
0.4	-	5K	(10.5 ,1.11 )	0.19
0	10 m	5K	(8.0 ,0.63 )	0.18
0	20 m	5K	(7.7,0.62 )	0.17
0	40 m	5K	(7.6 ,0.61 )	0.14
0.4	40 m	5K	(8.9,0.7 )	0.20
0	-	2.5K	(4.0 ,0.53 )	0.13
0	40 m	2.5K	(3.9 ,0.50 )	0.23
0.4	40 m	2.5K	(4.3,0.46 )	0.20

Table 5: Mean and variability of the Walker circulation in the spatially extended simulations.

#### 4. Spatially extended simulations with a warm pool

This section presents the results of spatially extended simulations for the  
395 stochastic multcloud model with non-uniform SST backgrounds, mimicking the  
Indian Ocean western Pacific warm pool (Section 2.4). Simulations with new  
mechanisms are considered and compared to FMK13, CRMs, and observations.  
We first consider separately variation of CRF and ocean layer depth before  
combining the effects. The results are summarized in Table 5.

400 The numerical method used is an operator-splitting strategy where the con-

servative terms are discretized and solved by a non-oscillatory central scheme while the remaining convective forcing terms are handled by a second-order Runge-Kutta method [57, 58]. As for the single column simulations, the stochastic component of the scheme is resolved using Gillespie’s exact algorithm [55].  
405 We consider the same parameter regimes discussed in the previous section and perform 800 day simulations, with a 5 minute time step and a resolution of 40 km.

#### 4.1. Variation of either CRF or ocean layer depth

In all we consider six distinct model configurations. In addition to FMK13,  
410 we present simulations with weak and strong CRF ( $\alpha = 0.1$  and  $0.4$  respectively). Separately, we consider addition of 10,20 and 40 meter deep ocean layer to FMK13. Figure 6 shows mean zonal vertical structure for all the regimes computed from 2000 days of data. We note that in all cases, an introduction of ocean layer decreases the strength of the zonal mean winds and makes  
415 the relative strength of the first baroclinic mode component stronger. The radiative convective feedback allows for slightly stronger circulation with higher second baroclinic component. For warm pool simulations, introduction of CRF increases strength and mean of the Walker cell by about 10 percent. The results are summarized in Table 5. The significant result here is low level cooling  
420 associated with the ocean coupling. The ocean acts as an energy sink and contributes to the weaker mean Walker circulation. This is in sharp contrast with counterintuitive result of [46], where the authors propose recharge-discharge theory to account for an increased heating associated with AOC. On the other hand anomaly effects on wind evaporation feedback are completely absent in  
425 the present models.

The Figure 7 shows deviations from zonal mean velocity field for all the regimes. We note that the simulations with the CRF produce the strongest intermittent bursts of convection. In particular the both weak and strong CRF ( $\alpha = 0.1$  and  $0.4$  respective) simulations in panels B and C are more intermittent  
430 than the FMK13 simulation in panel A. These simulations also produce the

strongest variability and mean, as shown in Table 5. The simulation with ocean (but without CRF), shown in figure D, shows an interesting low frequency variability on order of 100 days. The remnants of this behavior can be seen when a weak CRF is also introduced in panel E, but disappear with the stronger  
435 CRF of panel F.

Figure 8 shows Fourier spectrum for velocity, atmospheric moisture, ABL and sea surface temperature. We note that variability for the base FMK13 case, is characterized by 15 day convectively coupled waves. These are associated with synoptic systems originating inside of the warm pool. A similar oscillation is  
440 observed by [18] in a CRM study. The shallower ocean layer shifts the variability towards (particularly in atmospheric and ABL moisture) lower frequency time scales. A similar effect is associated with lower SST gradient discussed in the following section. In all cases, the ocean layer decreases the strength of the variability and introduces low frequency envelope structures in atmospheric and  
445 ocean boundary layer fields. The Fourier analysis in Figure 8 shows a progressive shift towards the lower frequencies associated with the increase in ocean depth. The same figure shows the effects of the CRF, which are mixed in nature. The lower values of CRF enhance the intrinsic low frequency oscillation while the higher values suppress them, as previously seen in column simulations of  
450 Section 3. The radiative convective feedback allows for slightly larger amplitude variability but negatively impacts low frequency oscillations in the system.

Note that, we omit spatially extended homogeneous SST simulations, since it is hard to distinguish (visually) the difference between standard FMK13 simulations and the ones with low and moderate radiative convective feedback. We  
455 also performed simulations with wind induced surface heat exchange (WISHE) [59]. Likewise, these results are also omitted, since the addition of WISHE mechanism did not appear to have a significant impact on the mean or the variability of the stochastic multcloud model simulations.

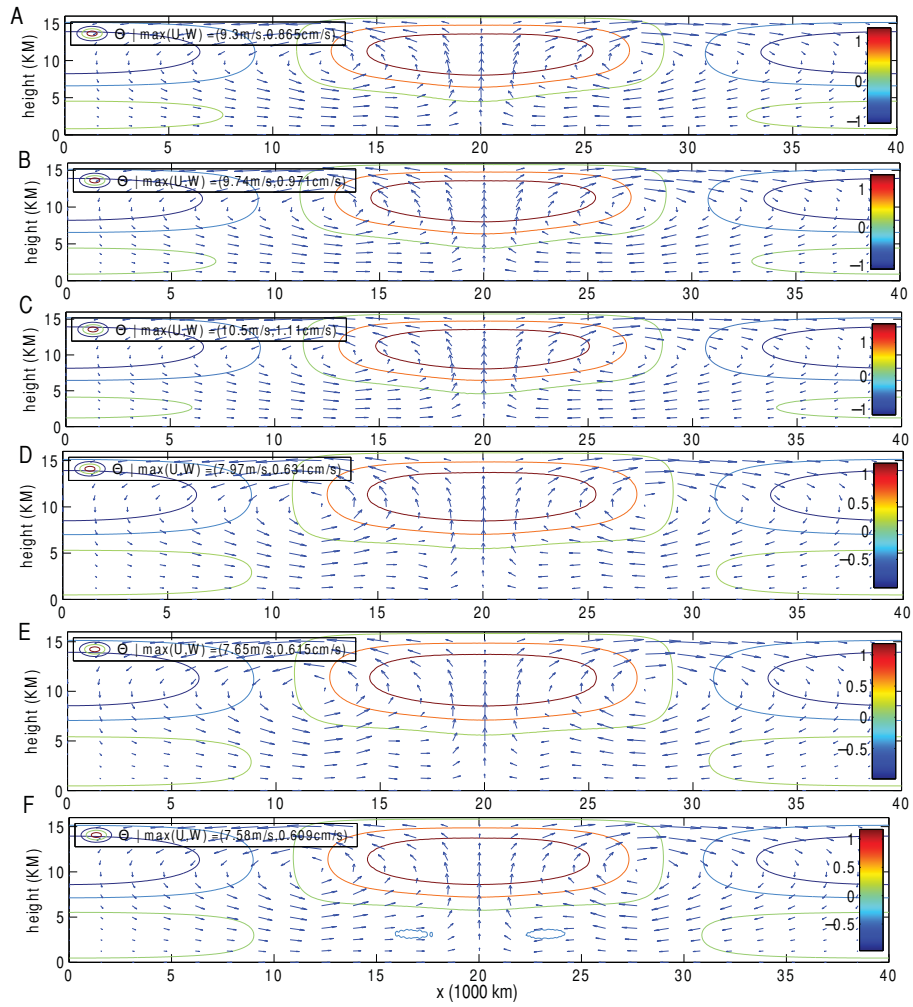


Figure 6: Mean zonal vertical structure associated with: A) FMK13 B) FMK13 with weak CRF C) FMK13 with strong CRF. D) FMK13 with 10 meter ocean , E) FMK13 with 20 meter ocean, F) FMK13 with 40 meter ocean .

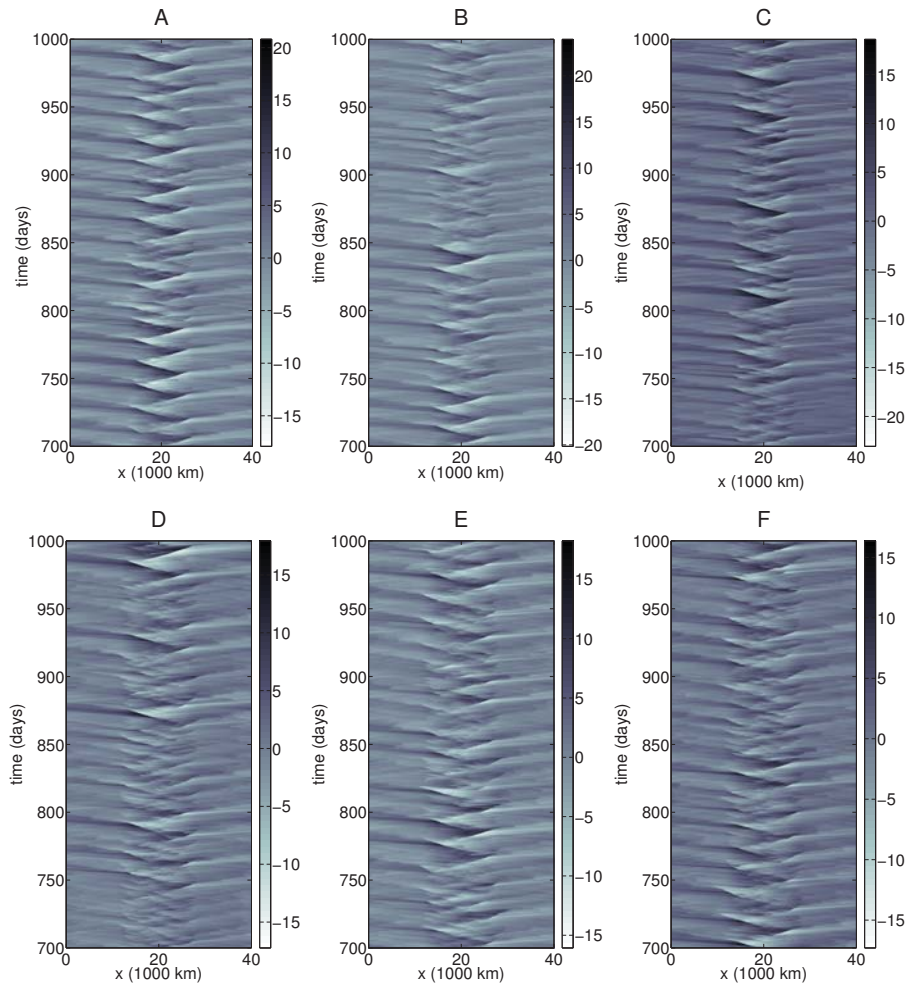


Figure 7: Contours of velocity anomalies  $u_1(x, t)$  for: a) FMK13, b) FMK13 with weak CRF, c) FMK13 with strong CRF, d) FMK13 with 10 meter ocean, e) FMK13 with 20 meter, f) FMK13 with 40 meter ocean. Anomalies are computed as deviations from the time-averaged mean state.

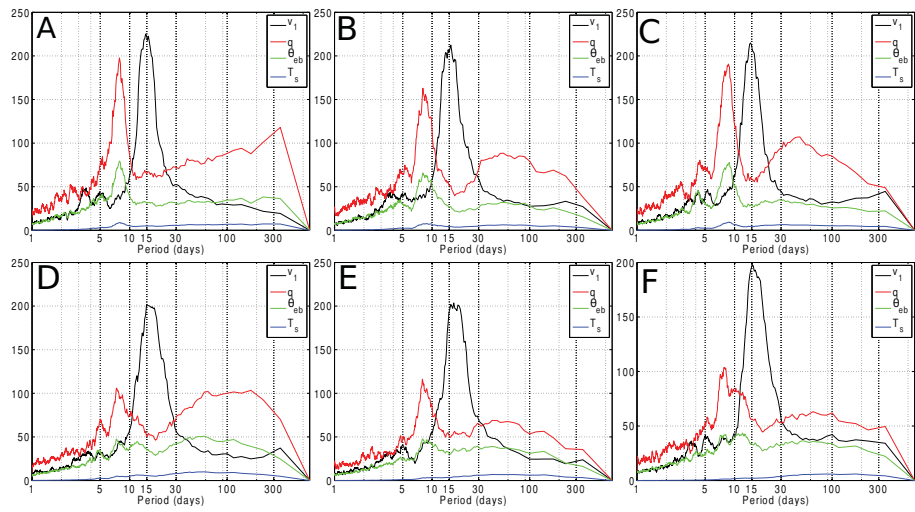


Figure 8: Power spectrum of the velocity from 500 days of observations at 20 equally spaced sites in the warm pool for simulations associated with a) FMK13, b) FMK13 with weak CRF, c) FMK13 with strong CRF, d) FMK13 with 10 meter ocean , e) FMK13 with 20 meter ocean, f) FMK13 with 40 meter ocean.

4.2. *Combining effects of cloud radiative feedback and atmosphere- ocean coupling*

460

Here we consider three distinct model CRF/AOC configurations :FMK13, FMK13 with ocean coupling , FMK13 with ocean coupling and weak  $\alpha = 0.1$  radiative feedback. In addition, we use warm pool strength of 5K (typical of multicloud models) and 2.5 K for each of three model configurations. Thus in total we consider six total parameter regimes, which highlight the combined effects of CRF and AOC, as well as SST strength.

465

To begin, we consider in the detail the dynamics of the spatially extended model with weak CRF and 40 meter ocean layer coupling in Figure 9. The contours of velocity field (upper left panel) show three large convective events in the center of the warm pool occurring in span of 50 days. The events are associated with build up of boundary layer moisture (lower left panel) which in turn appears to be coupled with the ocean temperature (middle left panel). These large convectively coupled waves have a high deep convective heating coupling and moisture content. They also produce faster convectively coupled gravity waves outside of the warm pool. These waves carry less moisture (lower right panel) but still produce intermittent deep convective events in the suppressed regions of the Walker circulation. We also observe a myriad of small amplitude standing wave activity in  $\theta_{eb}$  and  $T_S$  fields inside of the warm pool. These are associated with the congestus clouds that are responsible for the moistening of the mid-troposphere and preconditioning the system for the next convective event. The congestus heating is generally abundant inside of the positive SST area of the warm pool.

475

480

The Figure 10 show mean zonal vertical structure for all the regimes computed from 2000 days of data. We note that in all cases, ocean layer decreases the strength of the mean and make for more first baroclinic mode dominated circulation. The radiative convective feedback allows for slightly stronger circulation with higher second baroclinic component. For warm pool simulations, introduction of CRF increases strength and mean of the Walker cell by about 10 percent. Unsurprisingly, weaker SST gradient results in weaker mean circula-

485

490 tion. The effects of ocean coupling are also less drastic in the weak SST gradient case. In fact, the simulation with ocean and CRF mechanism is stronger than the FMK regime for 2.5K SST forcing.

More importantly, the weaker SST gradient fundamentally changes the frequency of the generation of the synoptic scale waves inside the warm pool. Figure 11 shows deviations from zonal mean velocity field for all the regimes. 495 The weaker 2.5K warm pool shifts the variability towards 30 day convectively coupled waves which have moisture and ABL temperature spectral peak near 150 days. Unlike the mean, the amplitude of the waves is not impacted by weaker SST gradient. The simulations with ocean and CRF mechanisms appear 500 more intermittent compared to FMK13 simulations. A remnant of the low frequency envelope can be seen in the ocean coupled simulations of panel B. This pattern is hard to discern visually when CRF is added in panel C.

In order to elucidate the low frequency dynamics in the system, we consider the Fourier spectrum for velocity, atmospheric moisture, ABL and sea surface 505 temperature in Figure 12. For both weak and strong SST gradient, the addition of ocean shifts the power spectrum towards the seasonal time scales. The results are mostly seen in ABL and atmospheric moisture while changes in velocity spectrum (as well as precipitation) are more subtle. Conversely, the introduction of the CRF shifts the spectrum towards marginally higher frequencies (moisture 510 spectrum in particular). The weaker SST gradient fundamentally alters the moisture spectrum: from bimodal to a single low frequency peak. This change in the moisture power spectrum likely indicates slower moisture build up inside of the warm pool and is responsible for the doubling of the period of generation of the synoptic scale disturbances inside of the warm pool.

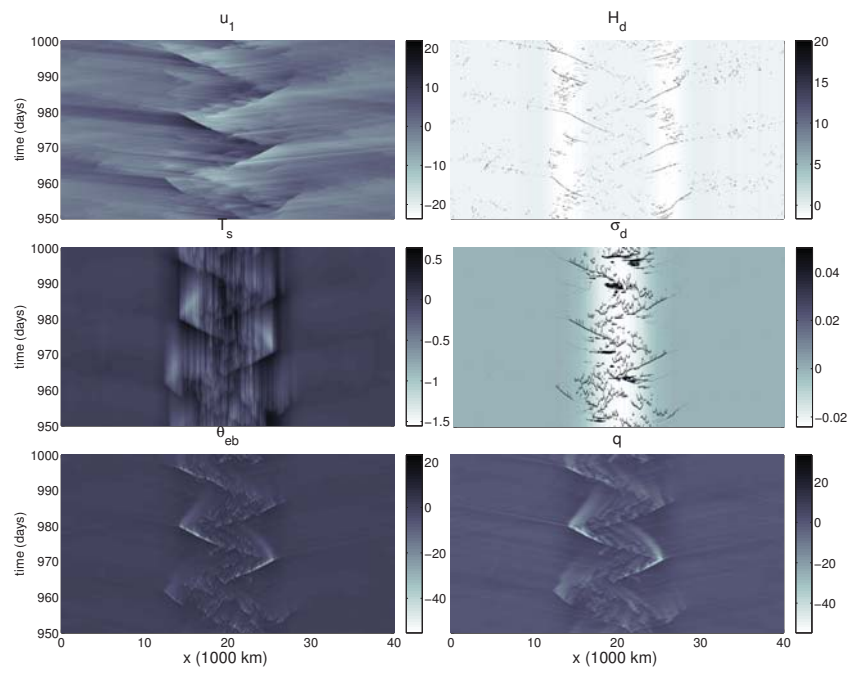


Figure 9: Hovmoller diagram showing 50 days of anomalies for stochastic multicloud model simulation with weak RCF and 40 meter deep ocean layer.

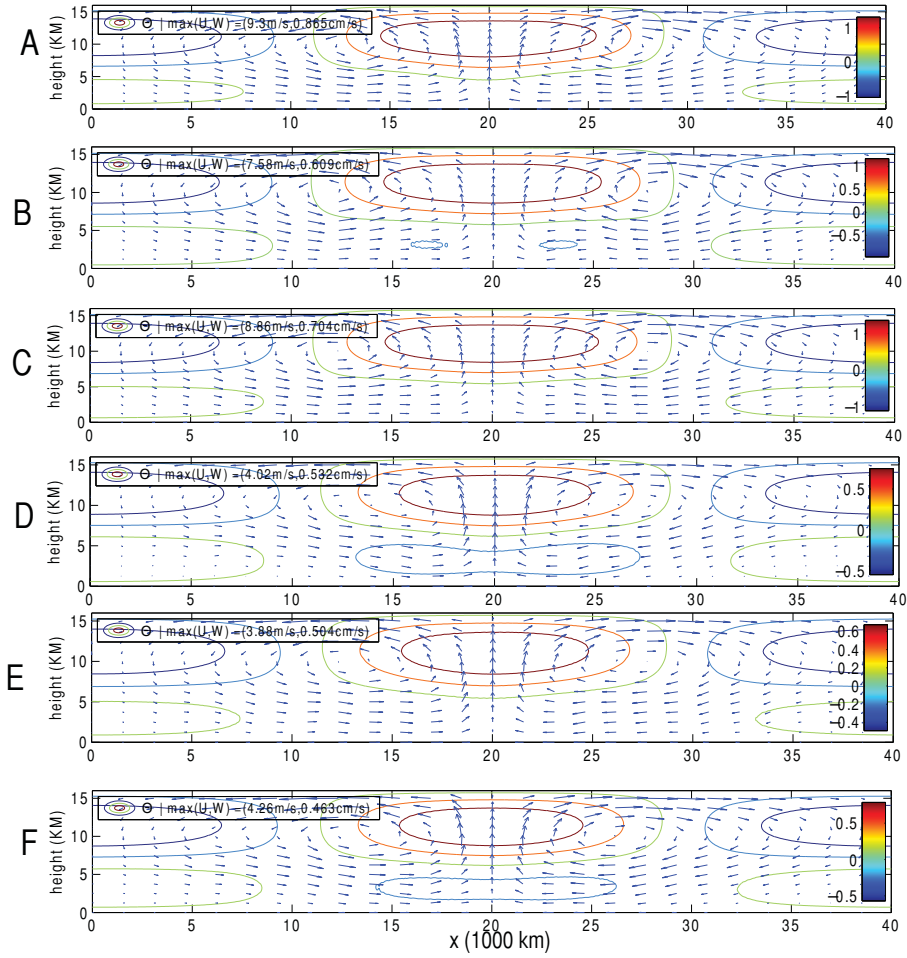


Figure 10: Mean zonal vertical structure associated with: A) FMK13 (5K warm pool), B) FMK13 with ocean coupling (5K warm pool), C) FMK13 with ocean coupling and radiative convective feedback and 2.5K warm pool, D) FMK13 (5K warm pool), E) FMK13 with ocean coupling and 2.5K warm pool, F) FMK13 with ocean coupling and radiative convective feedback 2.5K warm pool. Wherever appropriate, we use strong CRF and 20 meter ocean.

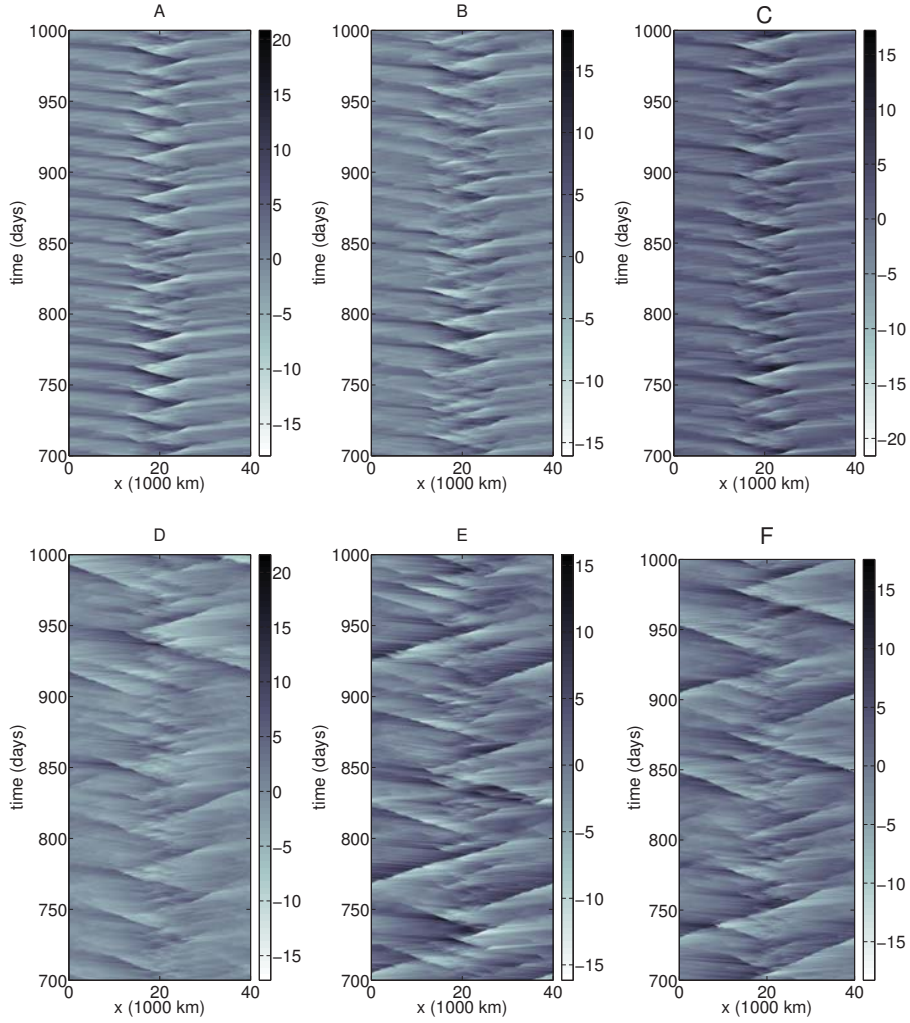


Figure 11: Contours of velocity anomalies  $u_1(x, t)$  for an interval of 300 days for: A) FMK13 (5K warm pool), B) FMK13 with ocean coupling (5K warm pool), C) FMK13 with ocean coupling and radiative convective feedback and 2.5K warm pool, D) FMK13 (5K warm pool), E) FMK13 with ocean coupling and 2.5K warm pool, F) FMK13 with ocean coupling and radiative convective feedback 2.5K warm pool. Wherever appropriate, we use strong CRF and 20 meter ocean. Anomalies are computed as deviations from the time-averaged mean state.

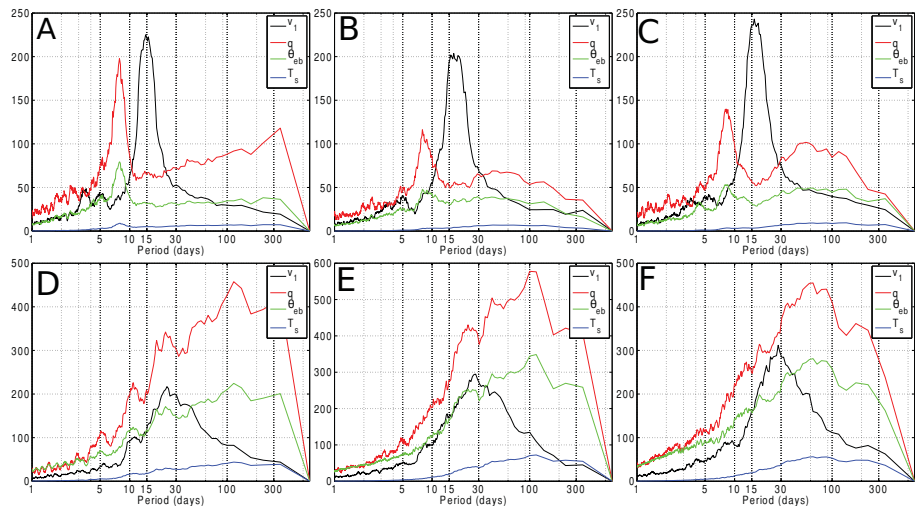


Figure 12: Power spectrum of the velocity from 500 days of observations at 20 equally spaced sites in the warm pool for simulations associated with: A) FMK13 (5K warm pool), B) FMK13 with ocean coupling (5K warm pool), C) FMK13 with ocean coupling and radiative convective feedback and 5K warm pool, D) FMK13 (2.5K warm pool), E) FMK13 with ocean coupling and 2.5K warm pool, F) FMK13 with ocean coupling and radiative convective feedback 2.5K warm pool. Wherever appropriate, we use strong CRF and 20 meter ocean.

515 **5. Conclusions**

Here, the stochastic multcloud model modified with new parameterized cloud radiation feedback and atmosphere-ocean coupling mechanisms is used to study horizontally homogeneous one column model dynamics and flows above the equator without rotation effects. The stochastic model is based on a coarse grained Markov chain lattice model where each lattice site takes discrete values from 0 to 3 according to whether the site is clear sky or occupied by a congestus, deep or stratiform cloud. The convective elements of the model interact with each other and with the large scale environmental variables through CAPE and middle troposphere dryness. The multcloud parameterization greatly improves the representation of the cloud distributions compared to the Betts-Miller scheme which typically are used for radiative feedback studies in coarse vertical resolution models [27, 5] and allows for results which rival the much more computationally complex GCM simulations [27]. The emphasis in this study is placed on elucidating the role intraseasonal and seasonal variability in the system.

In Sections 2.3 and 2.4, we propose simple parameterized closures for cloud radiation feedback and atmosphere ocean coupling. The basis for the CRF is an assumption that each cloud has a fixed radiative profile, with strength proportional to the cloud fraction in each computational grid point. Similarly, convective cloud fractions impact the ocean layer temperature by blocking proportional amount short-wave solar heating. In column simulations, the atmospheric ocean coupling introduces low frequency variability on the scale associated with ocean mixed layer depth. These intraseasonal and seasonal oscillations are characterized by periods of enhanced and suppressed convective activity corresponding to positive and negative ocean layer temperature anomalies. The enhanced phase of the oscillations is distinguished by abundance of organized convection. Similarly, to the suppressed phase of the MJO, the suppressed phase of the low frequency oscillation in the column model is characterized by small cloud coverage and intermittent deep convection.

545 In spatially extended simulations of Section 4, the radiative convective feed-  
back mechanism is shown to increase the mean and variability of Walker circula-  
tion. This increase in the variability is associated with low frequency convective  
features such as propagating synoptic scale systems originating inside of the en-  
hanced SST area. These are similar to the cycles observed in CRM simulations  
550 [18] but at a very small fraction of the computational cost. We use Fourier  
spectrum analysis to show that the ocean layer depth as well as the strength  
of the imposed SST gradient can be use to control the frequency of these low  
frequency convective features.

The study illustrates both the usefulness and limitation of the column model  
555 simulations for testing the mechanisms. Column simulations are essential in  
exploring parameter space and finding some of the catastrophic instabilities.  
However, the column simulations can easily exaggerate the impact of the studied  
mechanisms. In particular, it is clear that the intermediate and low frequency  
time scale features seen in the column simulations are distorted and to some  
560 extent neutralized by fast mixing by the horizontally propagating gravity waves  
in the spatially extended simulations.

Overall, the study develops and tests a systematic framework for incorpo-  
rating parameterized radiative cloud feedback and ocean coupling. The two  
mechanisms are are shown here to improve representation of intraseasonal and  
565 seasonal variability. This new variability has subtle effect on the mean state  
and precipitation statistics and has a great potential for interaction with other  
low frequency phenomena. These schemes can readily be implemented in deter-  
ministic and stochastic multcloud model GMC simulations[42, 43, 42, 44, 45],  
which already capture essential features low frequency features, such as MJO.

570 The research of S.N.S is partially supported by grants NSF DMS-1209409,  
ONR YIP N00014-12-1-0744, and ONR MURI N00014-12-1-0912. The research  
of A. J. M. is partially supported by National Science Foundation grants DMS-  
0456713, DMS-1025468 and by the office of Naval Research grants ONR DRI  
N0014-10-1-0554 and N00014-11-1-0306 and MURI award grant ONR-MURI N-  
575 000-1412-10912. Y. F. is a postdoctoral fellow supported through A.J.Ms above

NSF and ONR grants.

## Appendix A. Evaporative cooling at the sea surface

We recall that evaporation term  $E$ , discussed in Section 2.4 is given by

$$E = \frac{1}{\tau_e}(\theta_{eb}^*(T_s) - \theta_{eb}) \quad (\text{A.1})$$

where  $\tau_e$  is evaporative time scale and  $\theta_{eb}$  is the boundary layer equivalent potential temperature, and  $\theta_{eb}^*$  is the saturation boundary layer equivalent potential temperature given as a function of SST. According to Clausius-Clapeyron equation, the saturation equivalent potential temperature has form

$$\theta_{eb}^* = \theta_b \exp\left(\frac{L_v q^*(T_b)}{c_p T_b}\right) \quad (\text{A.2})$$

Here  $T_b$  is the boundary layer temperature,  $\theta_b$  is the boundary layer potential temperature,  $L_v$  is the latent heat of vaporization,  $q^*$  is the saturation specific humidity, and  $c_p$  is the heat capacity of dry air. Although  $L_v$  depends on temperature and  $c_p$  depends on moisture content, the variations are small and we assume that both are constants given in Table 1.

In (A.2),  $q^*(T)$  is the saturation specific humidity, which for an ideal gas is given by

$$q^* = \frac{e^*}{e^* + \frac{R_v}{R_d}(p - e^*)} \quad (\text{A.3})$$

Here  $R_v$  is the gas constant for water vapor,  $R_d$  is the gas constant for dry air,  $p$  is the pressure, and  $e^*$  is the saturation water vapor pressure. I will take  $R_v$  and  $R_d$  to have the constant values given in Table 1. I will also take  $p = p_s = 1000$  hPa, since the latent heat exchange takes place at the ocean surface. If we assume that  $L_v$  is constant, then the equation (A.3) can be integrated to give the following equation for  $e^*$ :

$$e^*(T) = e^*(T_{ref}) \exp\left(\frac{L_v}{R_v} \left[\frac{1}{T_{ref}} - \frac{1}{T}\right]\right) \quad (\text{A.4})$$

We therefore have  $\theta_{eb}^*$  as a function of  $T$  by using (A.2), (A.3), and (A.4). We approximate  $T_b$  and  $\theta_b$  in these equations with the SST  $T_s$ , and we assume  $L_v$  and  $c_p$  take the constant values listed in Table 1. (A.2), (A.3), and (A.4) take the form

$$\theta_{eb}^* = \theta_b \exp\left(\frac{L_v q^*(T_s)}{c_p T_s}\right) \quad (\text{A.5})$$

$$q^*(T_s) = \frac{e^*(T_s)}{e^*(T_s) + \frac{R_w}{R_d}(p - e^*(T_s))} \quad (\text{A.6})$$

$$e^*(T_s) = e^*(T_{ref}) \exp\left(\frac{L_v}{R_v} \left[\frac{1}{T_{ref}} - \frac{1}{T_s}\right]\right) \quad (\text{A.7})$$

600 The equations (A.5), (A.6), and (A.7) show nonlinear relationship between  $\theta_{eb}^*$  and  $T_s$ . It appears that  $\theta_{eb}^*$  rises by 5 K for 1K rise in  $T_s$ , in the range 20-35 K as seen in Figure A.13 ( taking  $T_{ref} = 301$  K). A linear approximation of this nonlinear relationship below

$$\theta_{eb}^* \approx 5T_s \quad (\text{A.8})$$

is used in the model computations.

- 605 [1] T. Nakazawa, Tropical super clusters within intraseasonal variation over the western pacific, J. Meteorol. Soc. Japan 66 (1974) 823–839.
- [2] H. H. Hendon, B. Liebmann, Organization of convection within the Madden–Julian oscillation, J. GEOPHYS. RES. 99 (1994) 8073–8084.
- [3] M. Wheeler, G. N. Kiladis, Convectively coupled equatorial waves: Analysis  
610 of clouds and temperature in the wavenumber-frequency domain, J. Atmos. Sci. 56 (3) (1999) 374–399.
- [4] J. M. Slingo, K. R. Sperber, J. S. Boyle, J. Ceron, M. Dix, B. Dugas, W. Ebisuzaki, J. Fyfe, D. Gregory, J. Gueremy, J. Hack, A. Harzallah, P. Inness, A. Kitoh, W. Lau, B. McAvaney, R. Madden, A. Matthews, T. N.  
615 Palmer, C. Parkas, D. Randall, N. Renno, Intraseasonal oscillations in 15

atmospheric general circulation models: results from an AMIP diagnostic subproject, *Climate Dynamics* 12 (1996) 325–357.

- [5] M. W. Moncrieff, E. Klinker, Organized convective systems in the tropical western Pacific as a process in general circulation models: A TOGA COARE case-study, *Quarterly Journal of the Royal Meteorological Society* 123 (1997) 805–827.
- [6] J. F. Scinocca, N. A. McFarlane, The variability of modeled tropical precipitation., *J. Atmos. Sci.* 61 (2004) 1993–2015.
- [7] W. K. M. Lau, D. E. Waliser, *Intraseasonal Variability in the Atmosphere-Ocean Climate System*, Springer-Verlag, 2005.
- [8] C. Zhang, Madden-Julian oscillation, *Reviews of Geophysics* 43 (2005) RG2003.
- [9] J.-L. Lin, G. N. Kiladis, B. E. Mapes, K. M. Weickmann, K. R. Sperber, W. Lin, M. C. Wheeler, S. D. Schubert, A. Del Genio, L. J. Donner, S. Emori, J.-F. Guerey, F. Hourdin, P. J. Rasch, E. Roeckner, J. F. Scinocca, Tropical intraseasonal variability in 14 IPCC AR4 climate models. Part I: Convective signals, *Journal of Climate* 19 (12) (2006) 2665–2690.
- [10] G. Stephens, P. Webster, Sensitivity of radiative forcing to variable cloud and moisture, *J. Atmos. Sc.* 36 (1979) 1542–1556.
- [11] R. D. Cess, G. L. Potter, M.-H. Zhang, J.-P. Blanchet, S. Chalita, R. Colman, D. A. Dazlich, A. D. del Genio, V. Dymnikov, V. Galin, D. Jerrett, E. Keup, A. A. Lacis, H. Le Treut, X.-Z. Liang, J.-F. Mahfouf, B. J. McAvaney, V. P. Meleshko, J. F. B. Mitchell, J.-J. Morcrette, P. M. Norris, D. A. Randall, L. Rikus, E. Roeckner, J.-F. Royer, U. Schlese, D. A. Sheinin, J. M. Slingo, A. P. Sokolov, K. E. Taylor, W. M. Washington, R. T. Wetherald, I. Yagai, Intercomparison and interpretation of climate feedback processes in 19 atmospheric general circulation models, *Geophysical Research* 95 (1990) 601–615.

- [12] R. D. Cess, M. H. Zhang, W. J. Ingram, G. L. Potter, V. Alekseev, H. W. Barker, E. Cohen-Solal, R. A. Colman, D. A. Dazlich, A. D. Del Genio, 645 M. R. Dix, V. Dymnikov, M. Esch, L. D. Fowler, J. R. Fraser, V. Galin, W. L. Gates, J. J. Hack, J. T. Kiehl, H. Le Treut, K. K.-W. Lo, B. J. McAvaney, V. P. Meleshko, J.-J. Morcrette, D. A. Randall, E. Roeckner, J.-F. Royer, M. E. Schlesinger, P. V. Sporyshev, B. Timbal, E. M. Volodin, 650 K. E. Taylor, W. Wang, R. T. Wetherald, Cloud feedback in atmospheric general circulation models: An update, 101 (1996) 12791.
- [13] S. Bony, K. A. Emanuel, On the Role of Moist Processes in Tropical Intraseasonal Variability: Cloud-Radiation and Moisture-Convection Feedbacks., *Journal of Atmospheric Sciences* 62 (2005) 2770–2789.
- 655 [14] M. E. Peters, B. Bretherton, A Simplified Model of the Walker Circulation with an Interactive Ocean Mixed Layer and Cloud-Radiative Feedbacks, *Journal of Climate* 18 (2005) 4216–4234.
- [15] B. Tian, V. Ramanathan, A simple moist tropical atmosphere model: The role of cloud radiative forcing, *Journal of Climate* 16 (12) (2003) 2086–2092.
- 660 [16] ECMWF, Proceedings ECMWF/CLIVAR Workshop on Simulation and Prediction of Intraseasonal variability with Emphasis on the MJO (2003) 3–6 November.
- [17] M. Moncrieff, M. Shapiro, J. Slingo, F. Molteni, Collaborative research at the intersection of weather and climate, *WMO Bulletin* 56 (2007) 204–211.
- 665 [18] J. Slawinska, O. Pauluis, A. J. Majda, W. W. Grabowski, Multiscale Interactions in an Idealized Walker Circulation: Mean Circulation and Intraseasonal Variability, *Journal of Atmospheric Sciences* 71 (2014) 953–971.
- [19] W. W. Grabowski, P. K. Smolarkiewicz, CRCP: A Cloud Resolving Convection Parameterization for modeling the tropical convecting atmosphere, 670 *Physica D Nonlinear Phenomena* 133 (1999) 171–178.

- [20] W. W. Grabowski, Coupling cloud processes with the large-scale dynamics using the cloud-resolving convection parameterization, *J. Atmos. Sci.* 58 (9) (2001) 978–997.
- [21] W. W. Grabowski, An improved framework for superparameterization, *J. Atmos. Sci.* 61 (15) (2004) 1940–1952.
- [22] D. Randall, M. Khairoutdinov, A. Arakawa, W. Grabowski, Breaking the cloud parameterization deadlock, *Bulletin of the American Meteorological Society* 84 (11) (2003) 1547–1564.
- [23] A. J. Majda, Multiscale models with moisture and systematic strategies for superparameterization, *J. Atmos. Sci.* 64 (7) (2007) 2726–2734.
- [24] Y. Xing, A. J. Majda, W. W. Grabowski, New efficient sparse spacetime algorithms for superparameterization on mesoscales, *Monthly Weather Review* 137 (12) (2009) 4307–4324.
- [25] J. Slawinska, O. Pauluis, A. J. Majda, W. W. Grabowski, Multi-scale interactions in an idealized walker circulation: Simulations with sparse space-time superparameterization, *Mon Weather Review* in press. doi: 10.1175/MWR-D-14-00082.1.
- [26] X. Wu, M. W. Moncrief, Long-Term Behavior of Cloud Systems in TOGA COARE and Their Interactions with Radiative and Surface Processes: Effects on the Energy Budget and SST, *Journal of Atmospheric Sciences* 58 (2000) 1155–1167.
- [27] D. Zurovac–Jevtik, S. Bony, K. A. Emanuel, On the Role of Clouds and Moisture in Tropical Waves: A Two-Dimensional Model Study, *Journal of Atmospheric Sciences* 63 (2005) 2140–2155.
- [28] B. Khouider, A. J. Majda, A simple multcloud parametrization for convectively coupled tropical waves. Part I: Linear analysis, *J. Atmos. Sci.* 63 (2006) 1308–1323.

- [29] B. Khouider, A. J. Majda, Multicloud convective parametrizations with crude vertical structure, *Theor. Comp. Fluid Dyn.* 20 (2006) 351–375.
- 700 [30] B. Khouider, A. J. Majda, A simple multicloud parametrization for convectively coupled tropical waves. Part II: Nonlinear simulations, *J. Atmos. Sci.* 64 (2007) 381–400.
- [31] B. Khouider, A. J. Majda, Equatorial convectively coupled waves in a simple multicloud model, *J. Atmos. Sci.* 65 (2008) 3376–3397.
- 705 [32] B. Khouider, A. J. Majda, Multicloud models for organized tropical convection: Enhanced congestus heating, *J. Atmos. Sci.* 65 (2008) 897–914.
- [33] B. Khouider, j. Biello, A. J. Majda, A stochastic multicloud model for tropical convection, *Comm. Math. Sci.* 8 (1) (2010) 187–216.
- [34] Y. Frenkel, A. J. Majda, B. Khouider, Using the stochastic multicloud model to improve tropical convective parameterization: A paradigm example, *J. Atmos. Sci.* 69 (3) (2012) 1080–1105.
- 710 [35] Y. Frenkel, B. Khouider, A. J. Majda, Stochastic and deterministic multicloud parameterizations for tropical convection, *Climate Dynamics* 41 (February 2013) 1527–1551.
- 715 [36] M. A. Katsoulakis, A. J. Majda, D. G. Vlachos, Coarse-grained stochastic processes for microscopic lattice systems, *Proceedings of the National Academy of Sciences of the United States of America* 100 (3) (2003) 782–787.
- [37] B. Khouider, A. J. Majda, M. A. Katsoulakis, Coarse-grained stochastic models for tropical convection and climate, *Proceedings of the National Academy of Science* 100 (2003) 11941–11946.
- 720 [38] A. J. Majda, C. Franzke, B. Khouider, An applied mathematics perspective on stochastic modelling for climate, *Philosophical Transactions of the Royal*

- Society A: Mathematical, Physical and Engineering Sciences 366 (1875)  
 725 (2008) 2427–2453.
- [39] Y. Frenkel, B. Khouider, A. J. Majda, Simple multcloud models for the diurnal cycle of tropical precipitation. Part I: Formulation and the case of the tropical oceans, *J. Atmos. Sci.* 68 (10) (2010) 2192–2207.
- [40] Y. N. Takayabu, Large-scale cloud disturbances associated with equatorial waves. part I: Spectral features of the cloud disturbances., *J. Meteor. Soc. Japan* 72 (1994) 433–448.  
 730
- [41] A. J. Majda, S. Stechmann, B. Khouider, Madden-Julian Oscillation analog and intraseasonal variability in a multcloud model above the equator, *Proceedings of the National Academy of Science* 104 (2007) 9919–9924.
- [42] B. Khouider, A. St-Cyr, A. J. Majda, J. Tribbia, The MJO and convectively coupled waves in a coarse-resolution GCM with a simple multcloud parameterization, *J. Atmos. Sci.* 68 (2) (2011) 240–264. doi: 10.1175/2010jas3443.1.  
 735 URL <http://dx.doi.org/10.1175/2010JAS3443.1>
- [43] Q. Deng, B. Khouider, A. J. Majda, The MJO in a coarse-resolution gcm with a stochastic multcloud parameterization, *J. Atmos. Sci.* (2014) in press doi:10.1175/JAS-D-14-0120.1.  
 740
- [44] R. S. Ajayamohan, B. Khouider, A. J. Majda, Realistic initiation and dynamics of the Madden-Julian Oscillation in a coarse resolution aquaplanet GCM, *Geophys. Res. Lett.* 40 (23) (2013) 6252–6257. doi:10.1002/2013gl058187.  
 745 URL <http://dx.doi.org/10.1002/2013GL058187>
- [45] R. S. Ajayamohan, B. Khouider, A. J. Majda, Simulation of monsoon intraseasonal oscillations in a coarse-resolution aquaplanet GCM, *Geophys. Res. Lett.* 41 (15) (2014) 5662–5669. doi:10.1002/2014gl060662.  
 750 URL <http://dx.doi.org/10.1002/2014GL060662>

- [46] A. H. Sobel, C. S. Bretherton, H. Gildor, M. E. Peters, Convection, cloud-radiative feedbacks and thermodynamic ocean coupling in simple models of the walker circulation (2004) 393–405.
- 755 [47] R. H. Johnson, T. M. Rickenbach, S. A. Rutledge, P. E. Ciesielski, W. H. Schubert, Trimodal characteristics of tropical convection, *Journal of Climate* 12 (8) (1999) 2397–2418.
- [48] B. E. Mapes, Convective inhibition, subgrid-scale triggering energy, and stratiform instability in a toy tropical wave model, *J. Atmos. Sci.* 57 (10)  
760 (2000) 1515–1535.
- [49] M. A. Katsoulakis, A. J. Majda, D. G. Vlachos, Coarse-grained stochastic processes and monte carlo simulations in lattice systems, *Journal of Computational Physics* 186 (1) (2003b) 250 – 278.
- [50] J. T. Kiehl, On the Observed Near Cancellation between Longwave and  
765 Shortwave Cloud Forcing in Tropical Regions, *J. Climate* 7 (1993) 559–565.
- [51] S. K. Cox, K. Griffith, Estimates of Radiative Divergence during Phase III of the GARP Atlantic Tropical Experiment Part I. Methodology., *Journal of Atmospheric Sciences* 35 (1979) 576–585.
- 770 [52] S. K. Cox, K. Griffith, Estimates of Radiative Divergence during Phase III of the GARP Atlantic Tropical Experiment: Part II. Analysis of Phase III Results., *Journal of Atmospheric Sciences* 36 (1979) 586–601.
- [53] C. Schumacher, R. A. Houze, I. Kraucunas, The tropical dynamical response to latent heating estimates derived from the TRMM Precipitation  
775 Radar, *Journal of Atmospheric Sciences* 61 (2004) 1341–1358.
- [54] K. Kikuchi, B. Wang, Diurnal precipitation regimes in the global tropics, *J. Climate* 21 (2008) 2680–2696.

- [55] D. T. Gillespie, An exact method for numerically simulating the stochastic coalescence process in a cloud., *J. Atmos. Sci.* 32 (1975) 1977–1989.
- 780 [56] D. T. Gillespie, Exact stochastic simulation of coupled chemical reactions, *The Journal of Physical Chemistry* 81 (25) (1977) 2340–2361.
- [57] B. Khouider, A. J. Majda, A non oscillatory balanced scheme for an idealized tropical climate model; Part I: Algorithm and validation, *Theoretical and Computational Fluid Dyn.* 19 (2005) 331–354.
- 785 [58] B. Khouider, A. J. Majda, A non oscillatory balanced scheme for an idealized tropical climate model; Part II: Nonlinear coupling and moisture effects, *Theoretical and Computational Fluid Dyn.* 19 (2005) 355–375.
- [59] A. J. Majda, M. G. Shefter, Models for Stratiform Instability and Convectively Coupled Waves., *Journal of Atmospheric Sciences* 58 (2001) 1567–  
790 1584.

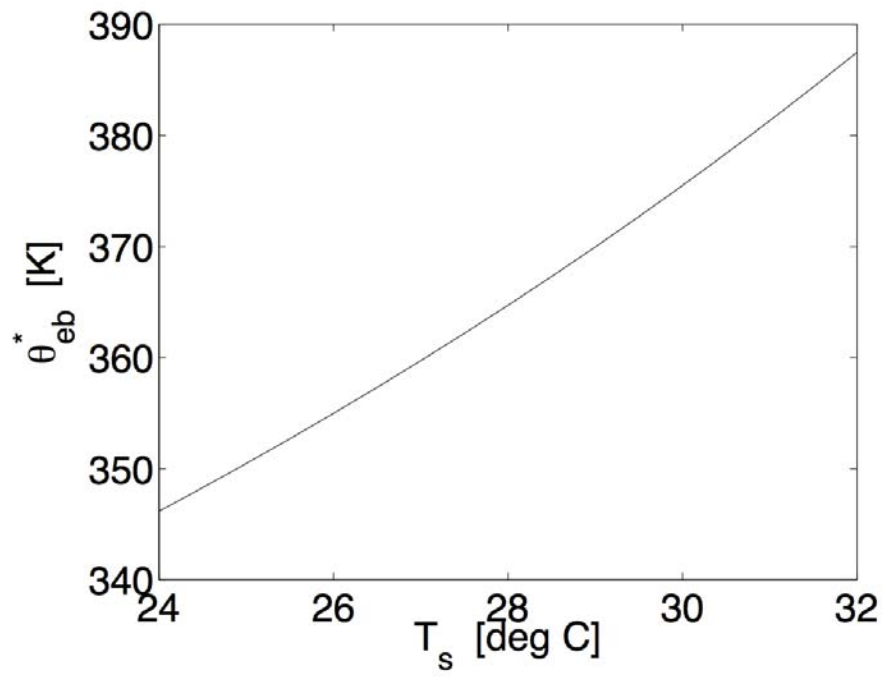


Figure A.13: The nonlinear relationship between  $\theta_{eb}^*$  and  $T_s$ . It appears that  $\theta_{eb}^*$  rises by 5 K for 1K rise in  $T_s$ . A linear approximation of this relationship is use in the model computations.